IGHEM 2000
July 10-12, 2000, Kempten, Germany

Flow Field Upstream of a Trash Rack Measured with an Acoustic Doppler Probe

Thomas Staubli, HTA Lucerne

Abstract

The flow field at the inlet of a small low head hydroelectric power plant was measured upstream of a trash rack using an acoustic Doppler probe. By integration of the multi-point measurements the time averaged discharge was calculated. Knowledge of the velocity and flow angle distributions upstream of the trash rack allowed to estimate local and integral energy losses. Furthermore, the flow field at the intake was statistically analyzed and turbulence intensity distributions were evaluated. Influences of upstream disturbances on the flow field, turbulence and vorticity distributions were quantified. Generally, knowledge of details of the inlet flow field to the turbines will be of interest if numerical flow computations for optimized turbine performance are planned in course of e.g. rehabilitation projects. In such cases, local acoustic velocity measurements provide accurate information with comparably little installation and measurement effort.

1. Acoustic Doppler Velocimeter (ADV)

The employed, commercially available acoustic probe permits to measure unsteady local 3D-velocity vectors. Acoustic sensing techniques (Figure 1) are used to measure flow in a sampling volume at a given distance from the transmitter and the receivers. The measured flow is therefore only to a minor degree disturbed by the presence of the probe. The instrument measures all three flow velocity components. The measurements are practically insensitive to water quality which allows for a wide range of applications.

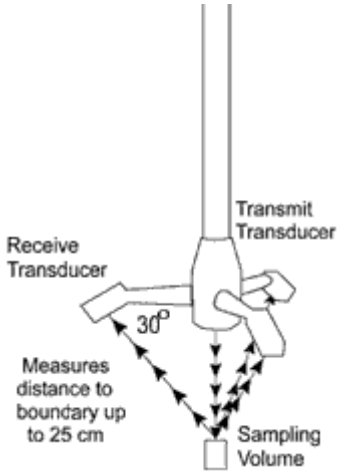

Figure 1. The Doppler velocity is derived from signals scattered by small particles in the sampling volume:
Velocity range is 2.5 m/s
Sampling rate of 25 Hz, (newer version 50 Hz),
Acoustic frequency 10 MHz,
Velocity resolution 0.1 mm/s, no zero-offset,
Sampling volume < 0.25 cm^3,
(Nortec AS, Norway).

The acoustic sensor consists of one transmit transducer and three receive transducers. The receive transducers are mounted on short arms around the transmit transducer at 120° azimuth intervals. The acoustic beams are oriented so that the receive beams intercept the transmit beam at a point located at 50 mm or 100 mm below the sensor. The interception of these four beams, together with the width of the transmit pulse, define the sampling volume.

ADV calibration factors are determined by the speed of sound and by the angles between the transmit and receive transducers. To ensure that the correct speed of sound is used, the water temperature and salinity must be entered in the data acquisition software. The calibration data were measured and provided by the manufacturer.

The velocity data were recorded to disk in compressed binary files which were further processed and analyzed using the LabVIEW-programming package (National Instruments).

2. Measurements

Measurements were performed at the inlet of the small hydroelectric power plant of Emmenweid in Lucerne built in 1934. These measurements were part of the final year project of the student Marcel Scheuber in 1999. The measuring plane was located 0.15 m upstream of the trash rack and had a cross section area of 23 m^2.

With the employed ADV probe unsteady velocity vectors were measured at 117 local points in the measuring plane, whereof 9 positions in depth and 13 positions in horizontal direction were chosen. The measuring points were more densely distributed near the walls and the free surface. For mounting and traversing the ADV probe a small carriage was constructed, which could be positioned at any immersion depth along the trash rack bars. Horizontally, the carriage had to be lifted manually to reach the desired positions.

Data were sampled over a period of one minute at a rate of 25 samples per second resulting in 1500 samples per measuring points. For each acquired data point all vector components as well as statistical information such as the correlation and standard deviation were stored.

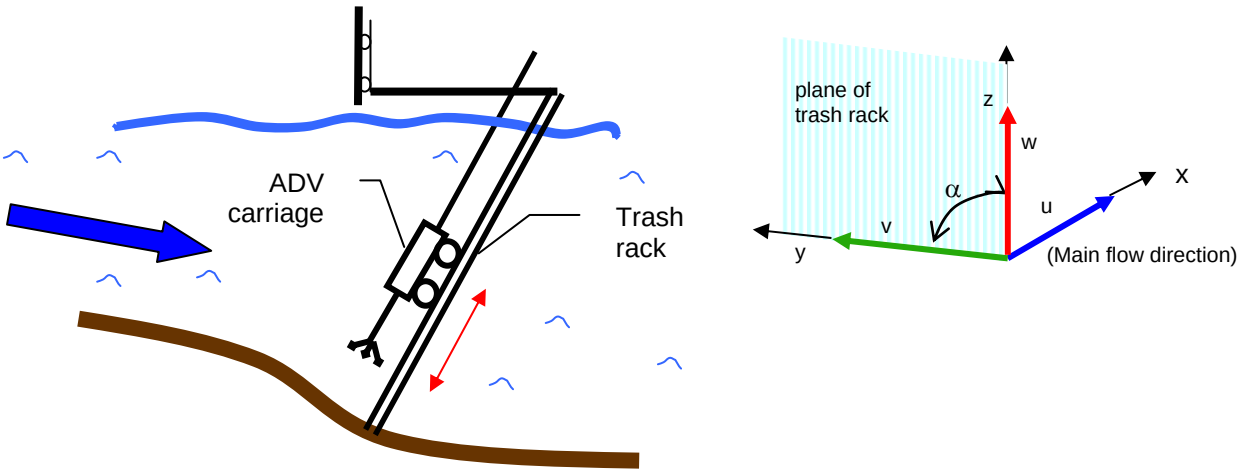

Figure 2. Schematic of the measuring setup and the used co-ordinate system

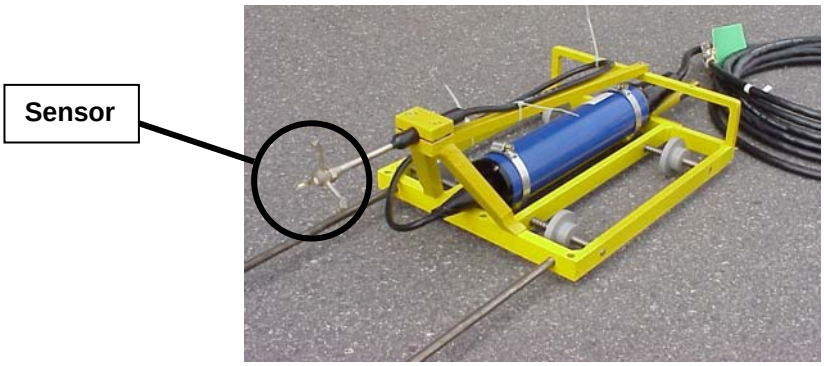

Figure 3. Photograph of the ADV carriage

3. Data processing

The raw data described above were further processed using LabVIEW programs. In a first step, the binary data files provided by the Nortek acquisition software were translated into ASCII files. Then the correlation of the samples were checked in a next step. The correlation parameter is provided by the ADV-software and is calculated on the basis of the normalized value of the covariance developed from the echo of the particles in the measuring volume, which is used to calculate the Doppler shift. If samples were detected which had correlation values below 0.7 then these samples were replaced by the time mean velocity values. Data quality was in general quite good so that only a few percent of the samples showed a correlation below this limit. Not eliminating data but replacing them by the average values made sure that uninterrupted time sequences of data were available for further analysis in the time and frequency domain.

A quantity of *n* discretely sampled data for the three velocity components were collected over the time period $T = n\Delta t$ at a sampling frequency $f_s = 1/\Delta t$:

$u_i, \quad v_i, \quad w_i$ sampled at $t_i = i\Delta t, \quad i = 0....n-1$

For data processing and analysis the following tools were made available using LabVIEW programs:

- **Mean values, standard deviations, higher order moments, and turbulence level evaluation**

Mean velocities:

$$\overline{u} = \frac{1}{n}\sum_{i=0}^{n-1} u_i \ , \quad \overline{v} = \frac{1}{n}\sum_{i=0}^{n-1} v_i \ , \quad \overline{w} = \frac{1}{n}\sum_{i=0}^{n-1} w_i$$ where *n* = number of samples

$$v_0 = \frac{1}{n}\sum_{i=0}^{n-1} \sqrt{u_i^2 + v_i^2 + w_i^2}$$

Standard deviation of the velocity components:

$$\sigma_u = \sqrt{\frac{1}{n}\sum_{i=0}^{n-1}\left(u_i - \overline{u}\right)^2} \ , \qquad \sigma_v = \sqrt{\frac{1}{n}\sum_{i=0}^{n-1}\left(v_i - \overline{v}\right)^2} \ , \qquad \sigma_w = \sqrt{\frac{1}{n}\sum_{i=0}^{n-1}\left(w_i - \overline{w}\right)^2}$$

Moment about the mean of the u-velocity component (analogous for the v- and w-components):

$\sigma_u^m = \frac{1}{n}\sum_{i=0}^{n-1}\left(u_i - \bar{u}\right)^m$ where m defines the order of the moment about the mean.

(m = 2→ variance = $\sigma_u^2 = \left(\sigma_u\right)^2$; m = 3 → skewness = $\frac{\sigma_u^3}{\left(\sigma_u\right)^3}$; m = 4 → kurtosis = $\frac{\sigma_u^4}{\left(\sigma_u\right)^4}$)

Turbulence level:

$$Tu = \frac{\sqrt{\frac{1}{3}\cdot\left(\sigma_u^2 + \sigma_v^2 + \sigma_w^2\right)}}{v_0}$$

- **Amplitude spectra, power spectra, phase spectra**

Amplitude spectra calculated with the discrete Fourier transform of the time sequences of n elements:

$U_k = \frac{1}{n}\sum_{i=1}^{n-1} u_i e^{-j2\pi ik/n}$ $V_k = \frac{1}{n}\sum_{i=1}^{n-1} v_i e^{-j2\pi ik/n}$ $W_k = \frac{1}{n}\sum_{i=1}^{n-1} w_i e^{-j2\pi ik/n}$ for *k* = 0, 1, 2, . . , *n*-1

The power spectra, providing information on spectral energy contents, are:

$S_{UU} = U_k U_k^*$ $S_{VV} = V_k V_k^*$ $S_{WW} = W_k W_k^*$

where * denotes the complex conjugate.

The cross power spectra yield to:

$S_{UV} = U_k^* V_k$ $S_{UW} = U_k^* W_k$ $S_{VW} = V_k^* W_k$

The phase spectra are showing the difference between the phases of two signals: e.g. the velocity components u_i and v_i or u_i and w_i (phase u_i minus phase v_i or minus w_i, respectively:

$\Phi_{UV} = \arctan\frac{\mathrm{Im}U_k}{\mathrm{Re}U_k} - \arctan\frac{\mathrm{Im}V_k}{\mathrm{Re}V_k}$ $\Phi_{UW} = \arctan\frac{\mathrm{Im}U_k}{\mathrm{Re}U_k} - \arctan\frac{\mathrm{Im}W_k}{\mathrm{Re}W_k}$

where Re is the real part and Im the imaginary part of the Fourier transforms.

- **Auto and cross correlation functions**

  (provides information on turbulent time and length scales)

$Ruu = \sum_{k=0}^{n-1} u_k u_{j+k}$ $Ruv = \sum_{k=0}^{n-1} u_k v_{j+k}$ $Ruw = \sum_{k=0}^{n-1} u_k w_{j+k}$

or $j = -(n-1), ..., -2, -1, 0, 1, 2, ..., m-1$

- **Coherence functions**

  (provides information on how closely the processes in x, y, z-direction are related)

$\Gamma_{uv}^2 = \frac{\left|S_{uv}\right|^2}{S_{uu}S_{vv}}$ $\Gamma_{uw}^2 = \frac{\left|S_{uw}\right|^2}{S_{uu}S_{ww}}$ $\Gamma_{vw}^2 = \frac{\left|S_{vw}\right|^2}{S_{vv}S_{ww}}$

Vorticity evaluation

The vorticity distribution in the y, z-plane was evaluated using the gradient of the interpolated velocity components in the trash rack plane.

$$\omega_x = \frac{\partial w}{\partial y} - \frac{\partial v}{\partial z}$$

Graphical representation of distributions

For graphical representation the data were linearly interpolated on the entire flow cross section. E.g. the normal velocity component for one point of turbine operation is displayed in Figure 4.

Discharge evaluation

Discharge $\dot{V} = \int u(y,z) \cdot dA = u_o A$ results from integration of the normal velocity component in the flow cross section. The area-averaged velocity u_o was calculated according ISO 3354:

Averaging of mean velocities on the horizontal line:

$$\begin{aligned} u_0 = u_{m1}\left[\frac{m_{fs}}{m_{fs}+1}e_1 + \frac{1}{12m_{fs}}\frac{e_2^{\,2}}{e_1} + \frac{7}{12}e_2 - \frac{1}{12}e_3\right] \\ + u_{m2}\left[\frac{1}{2}e_2 + \frac{7}{12}e_3 - \frac{1}{12}e_4\right] \\ + \sum_{i=3}^{i=n-2} u_{mi}\left[\frac{7}{12}\left(e_{(i+1)} + e_i\right) - \frac{1}{12}\left(e_{(i+2)} + e_{(i-1)}\right)\right] \\ + u_{(n-1)}\left[\frac{1}{2}e_n + \frac{7}{12}e_{(n-1)} - \frac{1}{12}e_{(n-2)}\right] \\ + u_{mn}\left[\frac{m}{m+1}e_{(n+1)} + \frac{1}{12m}\frac{e_n^{\,2}}{e_{(n+1)}} + \frac{7}{12}e_n - \frac{1}{12}e_{(n-1)}\right] \end{aligned}$$

Averaging of velocities on the vertical lines:

$$\begin{aligned} u_{mi} = u_1\left[\frac{m_{fs}}{m_{fs}+1}d_1 + \frac{1}{12m_{fs}}\frac{d_2^{\,2}}{d_1} + \frac{7}{12}d_2 - \frac{1}{12}d_3\right] \\ + u_{2m}\left[\frac{1}{2}d_2 + \frac{7}{12}d_3 - \frac{1}{12}d_4\right] \\ + \sum_{i=3}^{i=n-2} u_i\left[\frac{7}{12}\left(d_{(i+1)} + d_i\right) - \frac{1}{12}\left(d_{(i+2)} + d_{(i-1)}\right)\right] \\ + u_{(n-1)}\left[\frac{1}{2}d_n + \frac{7}{12}d_{(n-1)} - \frac{1}{12}d_{(n-2)}\right] \\ + u_n\left[\frac{m}{m+1}d_{(n+1)} + \frac{1}{12m}\frac{d_n^{\,2}}{d_{(n+1)}} + \frac{7}{12}d_n - \frac{1}{12}d_{(n-1)}\right] \end{aligned}$$

where e_i is the horizontal spacing of the measuring points and d_i the vertical spacing; m is the wall coefficient and m_{fs} the free surface coefficient.

3. Results

The overall duration for data acquisition of one turbine operating point was several hours. During this period discharge variations were monitored using a differential pressure measurement. In spite of minor discharge variations the mean discharge over the entire period was estimated to have a measuring uncertainty of less than ±1.5 percent. The integrated discharge of the velocity distribution of the operating point displayed in Figure 4 amounts to: $\dot{V} =$ 13.04 m^3/s.

The distribution of the normal velocity component in Figure 4 shows a velocity deficit in the center part due to the wake of an upstream pier. The backflow regions along the bottom boundary of the flow cross section indicate a badly designed intake.

The associated turbulence distribution shown in Figure 5 indicates in all backflow regions increased turbulence levels. Also in the wake flow the turbulence is obviously increased due to the vortex formation behind the pier. The same conclusion results also for the mean vorticity distribution displayed in Figure 6. Generally vorticity is increased in the boundary layers and in recirculation zones. The vorticity component ω_x evaluated in the y/z-plane can be interpreted as vortical structures

extending in streamwise direction. However, since these structures vary much with time it might be more insightful to evaluate the instantaneous vorticity from simultaneous measurement with more than one ADV probe.

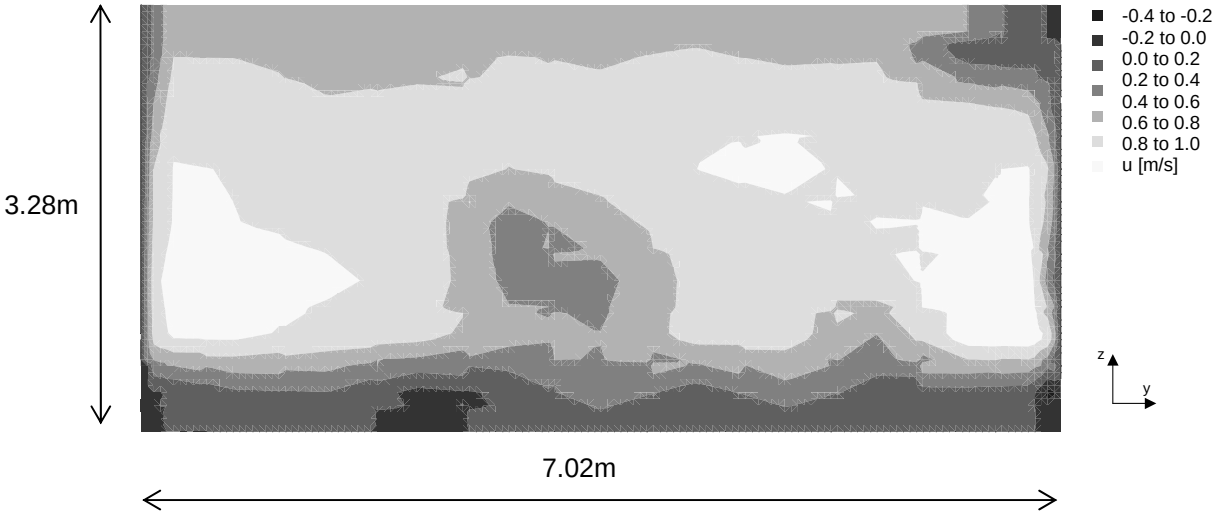

Figure . Normal velocity component *u(y,z)* in the plane of the trash rack (interpolated flow field, looking upstream)

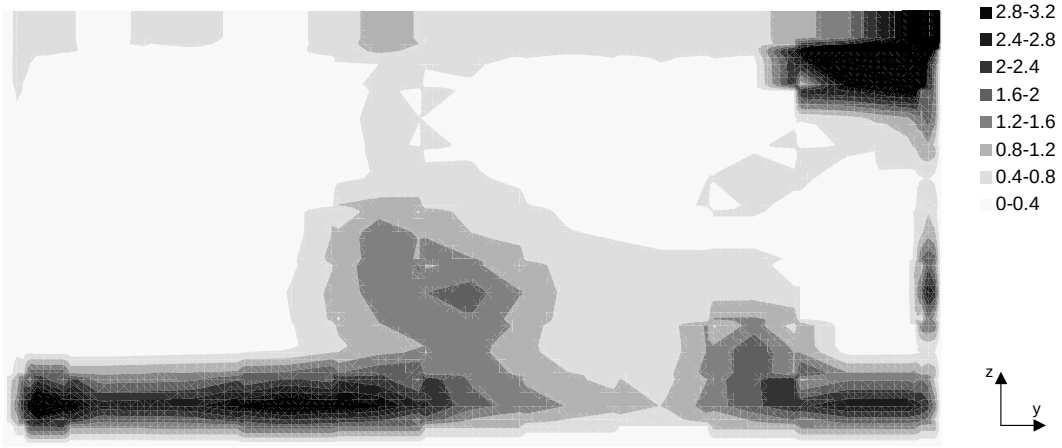

Figure 5. Turbulence intensity distribution *Tu(y,z)* measured in the plane of the trash rack

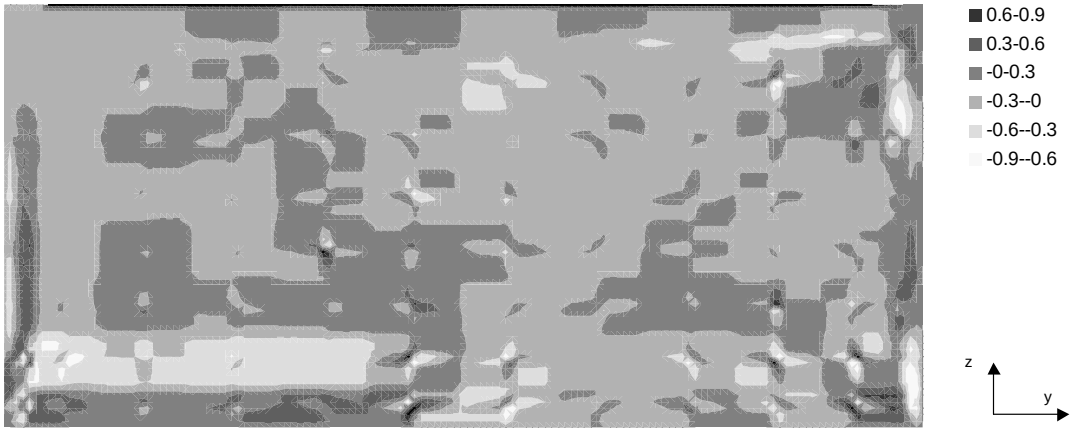

Figure 6. Vorticity distribution $\omega_x(y,z)$

An example analysis of a typical time signal of the center part of the flow cross section is shown in Figure 7. The power spectrum shows a distinct peak at a frequency of about 0.16Hz probably due to the vortex shedding behind the pier. The integral time scale can be estimated from the autocorrelation function to be about 0.5s. The regular vortex shedding with the frequency of 0.16Hz leads to an increase of the autocorrelation values at about 6.4s. Due to the dominantly stochastic character of the turbulent flow the autocorrelation function becomes very small for time delays of more than 10s.

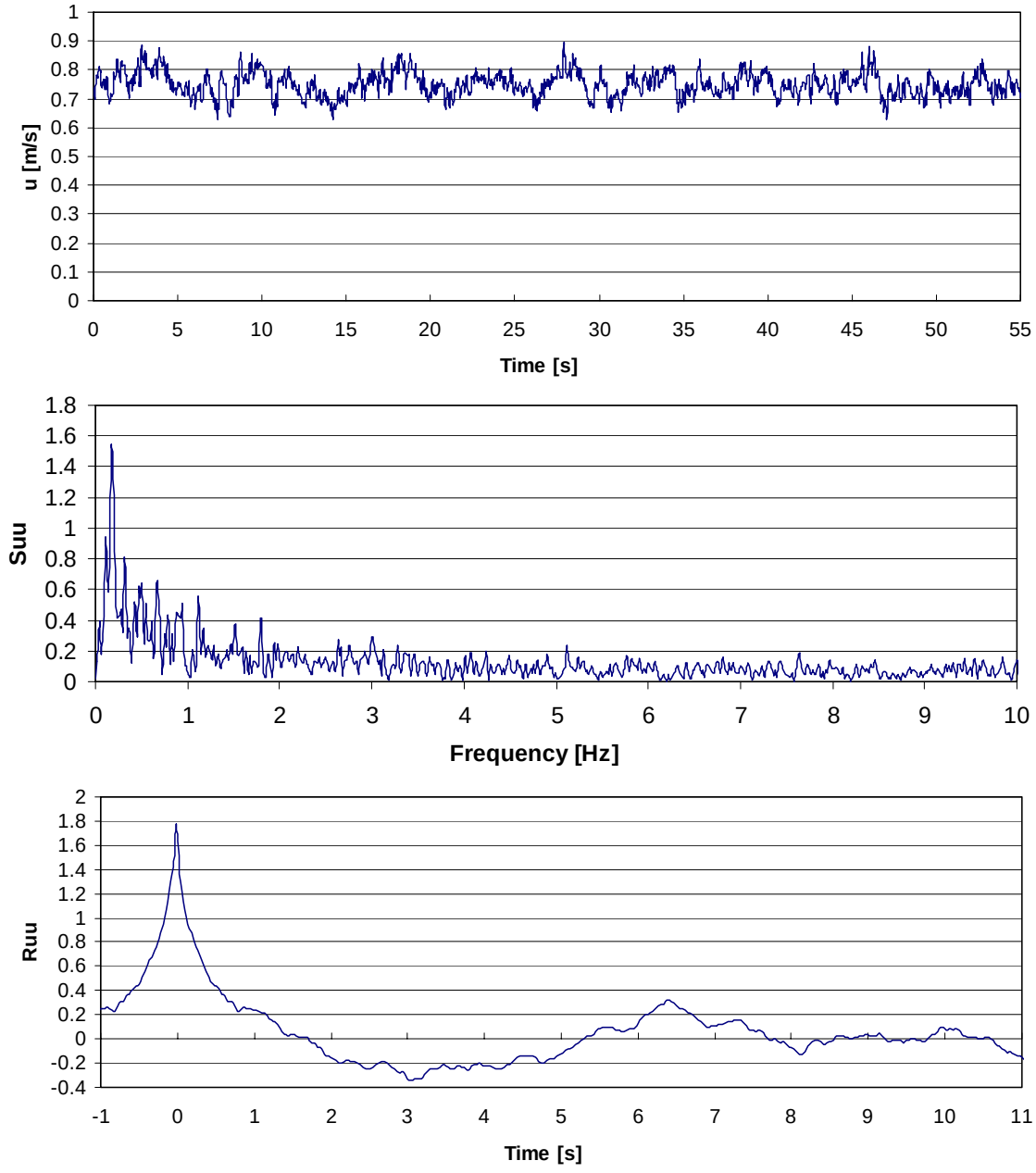

Figure 7. Example of a time signal, power spectrum and autocorrelation function for a typical measuring point in the center part of the flow cross section.

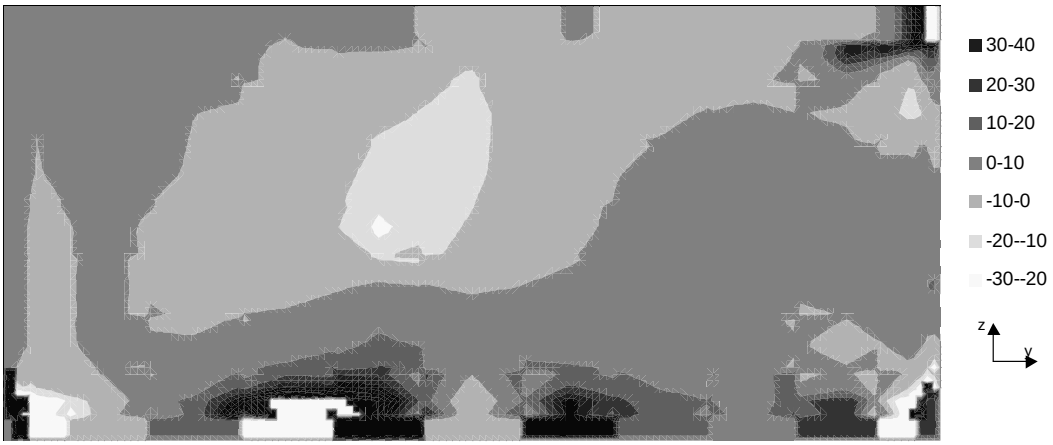

Figure 8. Incidence angles of the flow upstream of the trash rack: δ = *atan(v/u) [degree]*

The incidence angles of the flow shown in Figure 8 allows to estimate local trash rack losses. In the major part of the flow cross section this angle lies between ±10 degrees, which is in an acceptable range where trash rack losses do not increase by more than 10 percent. Locally however, in the recirculation zones and also in the wake of the pier, flow angles become much larger.

4. Conclusions

Measurements in the intake of a hydroplant using an acoustic Doppler velocity probe (ADV) showed to be a good way to measure discharge with little installation effort. The method might be especially of interest if for preparation of rehabilitation projects good discharge data are needed and if detailed knowledge of velocity distributions at the inlet supplies a decision basis for constructional modifications. The probe measurements provide detailed information on the flow field, its recirculation zones, turbulence characteristics, and deterministic phenomena like periodic vortex shedding. From local flow incidence to the trash rack good estimates of trash rack losses are possible. For acceptance tests the measuring accuracy is probably too low and the needed measuring time too high.

References

- Kirschmer, O., “Untersuchungen über den Verlust an Rechen”, Mitteil. Hydr. Inst München, No 1, 1926
- National Instruments Corporation, LabVIEW - Manuals, 1996
- Nortek AS, ADV Software Manual, 1998
- Scheuber, M., “Geschwindigkeitsverteilung vor dem Rechen einer Wasserkraftanlage”, HTA Lucerne, diploma thesis, 1999